

The quantum solvation, adiabatic versus nonadiabatic, and Markovian versus non-Markovian nature of electron transfer rate processes

Rui-Xue Xu,^{a)*} Ying Chen,^{a)} Ping Cui,^{a,b)} Hong-Wei Ke,^{b)} and YiJing Yan^{a,b)*}

^{a)}*Hefei National Laboratory for Physical Sciences at Microscale,*

University of Science and Technology of China, Hefei, Anhui, 230026, China

^{b)}*Department of Chemistry, Hong Kong University of Science and Technology, Kowloon, Hong Kong*

(Dated: February 1, 2008)

In this work, we revisit the electron transfer rate theory, with particular interests in the distinct quantum solvation effect, and the characterizations of adiabatic/nonadiabatic and Markovian/non-Markovian rate processes. We first present a full account for the quantum solvation effect on the electron transfer in Debye solvents, addressed previously in *J. Theore. & Comput. Chem.* **5**, 685 (2006). Distinct reaction mechanisms, including the quantum solvation-induced transitions from barrier-crossing to tunneling, and from barrierless to quantum barrier-crossing rate processes, are shown in the fast modulation or low viscosity regime. This regime is also found in favor of nonadiabatic rate processes. We further propose to use Kubo's motional narrowing line shape function to describe the Markovian character of the reaction. It is found that a non-Markovian rate process is most likely to occur in a symmetric system in the fast modulation regime, where the electron transfer is dominant by tunneling due to the Fermi resonance.

I. INTRODUCTION

A. Prelude

Electron transfer (ET) is the simplest reaction system but plays a pivotal role in many chemical and biological processes. The field of ET research has grown enormously since 1950s.^{1,2,3,4,5,6,7,8,9,10,11,12,13,14,15,16,17,18,19,20,21} The standard ET system-bath model Hamiltonian reads

$$H_T = h_a |a\rangle\langle a| + (h_b + E^\circ) |b\rangle\langle b| + V(|a\rangle\langle b| + |b\rangle\langle a|). \quad (1)$$

Here, E° denotes the reaction endothermicity, V the transfer coupling matrix element, and h_a (h_b) the solvent Hamiltonian for the ET system in the donor (acceptor) state. The system is initially in the donor $|a\rangle$ site, with the solvent (bath) equilibrium density matrix $\rho_a^{\text{eq}} \propto e^{-h_a/(k_B T)}$ at the specified temperature T .

The ET system of eq 1 can be treated as a spin-boson problem in the context of quantum dissipation. We have recently constructed a general theory of quantum dissipation,^{22,23,24} which results in an analytical solution to the ET dynamics in a Debye (solvent) dissipation.^{25,26} It is noticed that the exact construction leads always to a generalized rate equation:^{25,26,27}

$$\dot{P}_a(t) = - \int_0^t d\tau \hat{k}(t-\tau) P_a(\tau) + \int_0^t d\tau \hat{k}'(t-\tau) P_b(\tau). \quad (2)$$

Here, $\hat{k}(t)$ and $\hat{k}'(t)$ denote the forward and backward rate memory kernels. On the other hand, one often finds in practice that the simple kinetic theory, with a Markovian rate constant description, can well describe the observed rate process. The resulting reactant population $P_a(t)$ decays exponentially toward its equilibrium value at a given temperature. Note that formally the rate constant is just the integrated rate kernel over time. Is there

any quantitative justification for the Markovian rate processes being often observed experimentally? In this work, we try to address this issue, along with the quantum solvation effect and the adiabatic versus nonadiabatic nature of ET rate processes.

B. Background

Previous work on ET theory focuses mainly on the rate constant description. Consider Fig. 1, the schematics of the simple donor-acceptor ET system of eq 1. Here, the relevant (macroscopic) solvent potential surfaces V_a and V_b are plotted as the functions of solvation coordinate $U \equiv h_b - h_a$. The solvation energy for the ET from the donor $|a\rangle$ to the acceptor $|b\rangle$ site is given by^{1,2,3}

$$\lambda \equiv \text{tr}_B (U \rho_a^{\text{eq}}) \equiv \langle U \rangle. \quad (3)$$

The second identity here defines the notation $\langle \cdots \rangle$ for the bath ensemble average, where the trace runs over all the solvent (bath) degrees of freedom. At the crossing ($U + E^\circ = 0$) point, $V_a = V_b = (E^\circ + \lambda)^2/(4\lambda)$. It is the celebrated Marcus' ET reaction barrier height.^{1,2,3} Thus, Fig. 1 also summarizes the Marcus' nonadiabatic rate expression,

$$k_{\text{NA}} = \frac{V^2/\hbar}{\sqrt{\lambda k_B T/\pi}} \exp \left[- \frac{(E^\circ + \lambda)^2}{4\lambda k_B T} \right]. \quad (4)$$

This rate (constant) can be derived readily from eq 1, by using the classical or static Franck-Condon approximation, followed by the classical fluctuation-dissipation theorem, $\langle U^2 \rangle - \langle U \rangle^2 = 2k_B T \lambda$. It does not consider the *dynamic* solvation effect, which is characterized by the relaxation time and also associated with the viscosity of the solvent.^{11,12,13,14,15,16} Such effect was first studied by Kramers in his classical Fokker-Planck-equation approach to the rate theory of isomerization reaction.²⁸

The resulting rate shows the celebrated turnover behavior that the rate has a maximum in an intermediate viscosity region.^{28,29} This clearly demonstrates the dual role of solvent on reaction rate. Note that in the Kramers' rate theory, the reaction system is treated as a Brownian particle moving on a single adiabatic double-well potential surface.

The dynamic solvation on nonadiabatic ET has been incorporated in the quantum extension of Marcus' theory, formulated via the Fermi golden rule.^{18,19,20,21} The solvation coordinator is now a time-dependent stochastic operator $U(t) \equiv e^{i\hat{H}_a t/\hbar} U e^{-i\hat{H}_a t/\hbar}$, and assumed to follow the Gaussian statistics. Thus, the dynamic solvation is completely characterized by the correlation function,

$$C(t - \tau) = \langle [U(t) - \lambda][U(\tau) - \lambda] \rangle. \quad (5)$$

The Fermi-golden-rule formalism is valid for an arbitrary form of the solvation correlation function. But like the Marcus' theory, it is restricted in the second-order transfer coupling regime. The resulting rate does not show the Kramers' fall-off behavior^{28,29} that involves the barrier recrossing and thus depends on higher-order transfer coupling. The improved approach has been proposed, on the basis of the fourth-order perturbation theory, followed by certain resummation schemes.^{8,9,10,11,12,13,14,15,16,17,30} The resulting rate does support a smooth transition between nonadiabatic and adiabatic ET reaction, recovering properly the Kramers' turnover behavior.^{28,29}

In this work, we adopt the reduced density matrix dynamics approach that is closely related to our recent development of quantum dissipation theory.^{22,23,24} With the aid of the analytical expression for the nonperturbative and non-Markovian ET rate,^{25,26} we will elaborate in detail the quantum solvation effects in both the adiabatic and nonadiabatic reaction regimes, and further investigate their relations to the Markovian versus non-Markovian nature of ET reaction kinetics.

The remainder of this paper is organized as follows. Section II reviews the generalized kinetic rate theory, constructed readily via the reduced density matrix dynamics. In Sec. III we decompose the total rate into its adiabatic and nonadiabatic components, and also analyze the Markovian versus non-Markovian nature of population transfer dynamics. We propose to use the Kubo's motional narrowing function, originally used in the context of optical spectroscopy,^{31,32} to characterize the Markovian character of ET rate process. Section IV presents a full account of the effect of quantum versus classical solvation on some representative ET reaction systems. Section V analyses the population transfer dynamics, with the focus on their adiabatic/nonadiabatic and Markovian/non-Markovian characters. Finally, Sec. VI concludes the paper.

II. NON-MARKOVIAN RATES: THEORY

A. Generalized rate theory and dissipation

Let us define the dynamic rates via the evolution of reduced system density matrix ρ . In the absence of time-dependent external field, the generalized quantum master equation reads,

$$\dot{\rho}(t) = -i\mathcal{L}\rho(t) - \int_0^t d\tau \hat{\Pi}(t - \tau)\rho(\tau). \quad (6)$$

$\mathcal{L}\rho \equiv \hbar^{-1}[H, \rho]$, with $H \equiv \langle H_T \rangle$ being the reduced system Hamiltonian; $\hat{\Pi}(t - \tau)$ denotes the dissipation kernel. Note that eq 6 is formally exact; in fact, the involving nonperturbative $\hat{\Pi}(t)$ can be generally expressed in terms of continued fraction formalism.^{23,33,34}

To obtain the dynamic rates, we shall eliminate the coherent components ρ_{jk} ; $j \neq k$, from eq 6, and retain the populations $P_j(t) \equiv \rho_{jj}(t)$ only. To do that, let us recast eq 6 in its Laplace frequency-domain resolution,

$$s\tilde{\rho}(s) - \rho(0) = -[i\mathcal{L} + \Pi(s)]\tilde{\rho}(s), \quad (7)$$

and then arrange it into the block matrix form for the population and coherence vectors, $\tilde{\mathbf{P}} = \{\tilde{\rho}_{jj}\}$ and $\tilde{\mathbf{C}} = \{\tilde{\rho}_{jk}; j \neq k\}$, with $\mathbf{C}(t = 0) = \mathbf{0}$, respectively. We have

$$s\tilde{\mathbf{P}}(s) - \mathbf{P}(0) = -\mathbf{T}_{PP}(s)\tilde{\mathbf{P}}(s) - \mathbf{T}_{PC}(s)\tilde{\mathbf{C}}(s), \quad (8a)$$

$$s\tilde{\mathbf{C}}(s) = -\mathbf{T}_{CP}(s)\tilde{\mathbf{P}}(s) - \mathbf{T}_{CC}(s)\tilde{\mathbf{C}}(s), \quad (8b)$$

with the transfer matrices, \mathbf{T}_{PP} , \mathbf{T}_{PC} , \mathbf{T}_{CP} , and \mathbf{T}_{CC} , arising from the corresponding rearrangement of $i\mathcal{L} + \Pi(s)$. Eliminating the coherent component $\tilde{\mathbf{C}}$ leads to

$$s\tilde{\mathbf{P}}(s) - \mathbf{P}(0) = \mathbf{K}(s)\tilde{\mathbf{P}}(s), \quad (9a)$$

or, equivalently,

$$\dot{P}_j(t) = \sum_k \int_0^t d\tau \hat{K}_{jk}(t - \tau)P_k(\tau). \quad (9b)$$

The involving rate resolution matrix is obtained as

$$\mathbf{K}(s) \equiv \int_0^\infty dt e^{-st} \hat{\mathbf{K}}(t) = \mathbf{T}_{PC}(s + \mathbf{T}_{CC})^{-1} \mathbf{T}_{CP} - \mathbf{T}_{PP}. \quad (10)$$

Its element $K_{jk}(s)$ resolves the state-to-state dynamic rate memory kernel $\hat{K}_{jk}(t)$. The rate matrix satisfies the relation $\sum_j K_{jk} = 0$, as inferred from the population conservation, $\text{Tr}\rho = \sum_j P_j = \text{constant}$.

B. Generalized rate theory in the two-state system

For the two-state ET system (cf. eq 1 and Fig. 1) of present study, only a single dynamic rate equation is independent. That is eq 2, which reads in the Laplace domain as

$$s\tilde{P}_a(s) - P_a(t = 0) = -k(s)\tilde{P}_a(s) + k'(s)\tilde{P}_b(s). \quad (11)$$

Here, $k(s) \equiv L\{\hat{k}(t)\} = -K_{aa}(s)$ and $k'(s) \equiv L\{\hat{k}'(t)\} = K_{ba}(s)$ are the forward and backward rate resolutions, respectively. The involving transfer matrices for the simple ET system of eq 1 have all been identified; cf. the eqs 32 of Ref. 25:

$$T_{PP} = 0, \quad T_{PC} = \frac{iV}{\hbar} \begin{bmatrix} -1 & 1 \\ 1 & -1 \end{bmatrix}, \quad (12a)$$

$$T_{CP} = \begin{bmatrix} -iV/\hbar & z^* + iV/\hbar \\ iV/\hbar & z - iV/\hbar \end{bmatrix}, \quad (12b)$$

$$T_{CC} = \begin{bmatrix} x^* - i(E^\circ + \lambda)/\hbar & y^* \\ y & x + i(E^\circ + \lambda)/\hbar \end{bmatrix}. \quad (12c)$$

Here,

$$x \equiv \Pi_{ba,ba}, \quad y \equiv \Pi_{ba,ab}, \quad z \equiv \Pi_{ba,bb}, \quad (13)$$

and their complex conjugates $\Pi_{jj',kk'}^* = \Pi_{j'j,k'k}$ are the only nonzero elements of the Π -tensor. Denote also

$$\alpha(s) \equiv s + x(s) + (i/\hbar)(E^\circ + \lambda). \quad (14)$$

The final expressions for the rate resolutions are then²⁵

$$k(s) = \frac{2|V|^2}{\hbar^2} \text{Re} \left\{ \frac{\alpha(s) + y(s)}{|\alpha(s)|^2 - |y(s)|^2} \right\}, \quad (15a)$$

and

$$k'(s) = \frac{2|V|^2}{\hbar^2} \text{Re} \left\{ \frac{[\alpha(s) + y(s)][1 - i\hbar z^*(s)/V]}{|\alpha(s)|^2 - |y(s)|^2} \right\}. \quad (15b)$$

The involving parameters, defined in eq 13, can in principle be evaluated in terms of continued fraction formalism of the nonperturbative dynamics of reduced density matrix.^{23,33,34} In particular, the continued fraction expressions of these parameters have been solved analytically for the Debye solvent model, where the solvation correlation assumes a single exponential form.²⁵

III. NATURE OF RATE PROCESSES: ADIABATIC VERSUS NONADIABATIC AND MARKOVIAN VERSUS NON-MARKOVIAN

A. Adiabatic–nonadiabatic rate decomposition

It is noticed that the ET in the short-time ($t < \hbar/V$) regime is always nonadiabatic, or $k \propto V^2$. This fact can be inferred from the observation that the backscattering events, responsible by the higher-order transfer coupling, are yet not to occur. In Appendix A, we solve eqs 8 and 12 in the weak transfer coupling limit, and obtain the nonadiabatic counterpart of eq 15.

$$k_{NA}(s) = \frac{2V^2}{\hbar^2} \text{Re} \int_0^\infty dt \exp[-st - g(t)], \quad (16a)$$

with

$$g(t) = \frac{i}{\hbar}(E^\circ + \lambda)t + \frac{1}{\hbar^2} \int_0^t d\tau \int_0^\tau d\tau' C(\tau'). \quad (16b)$$

The corresponding $k_{NA}(s = 0)$ is the well established quantum nonadiabatic rate expression.^{8,9,10,11,12,13,14,15,16,17,18,19,20,21,30} The Marcus' expression, eq 4, can be obtained via setting $C(t) \approx C(0) = 2\lambda k_B T$ that amounts to the static (slow-modulation) approximation, followed by the classical fluctuation-dissipation theorem.

Consider now the long-time regime, involving only the integrated rate kernel, i.e., the rate constant $k \equiv k(s = 0)$ or $k' \equiv k'(s = 0)$. Hereafter, rate constant will be referred in short as rate if it causes no confusion. For the later use, denote also the reaction equilibrium constant,

$$K_{eq} = \frac{P_b(\infty)}{P_a(\infty)} = \frac{k(s = 0)}{k'(s = 0)} \equiv \frac{k}{k'}. \quad (17)$$

It is noticed that $k \leq k_{NA}$ is expected to hold in general; see Fig. 6 and its comments followed, especially on the case of exception. This inequality may be inferred from the fact that the total k contains the backscattering contributions, while the nonadiabatic k_{NA} does not. The decomposition of the total rate into its nonadiabatic and adiabatic components may therefore be introduced as^{11,12,13,14,15,16}

$$\frac{1}{k} = \frac{1}{k_{NA}} + \frac{1}{k_A}. \quad (18)$$

As k and k_{NA} can be evaluated via eq 15a and eq 16, respectively, with $s = 0$, the above equation can in fact be considered as the working definition of adiabatic k_A . We shall show later that k_A is relatively much insensitive (compared with k_{NA}) to the transfer coupling strength V variable (cf. Fig. 5). Therefore, it can be practically used to describe the adiabatic rate process that involves only the ground solvation surface via the diagonalization of eq 1. The ratio k_{NA}/k_A can be considered as the adiabaticity parameter. The ET reaction assumes adiabatic when $k_{NA}/k_A \gg 1$, and nonadiabatic when $k_{NA}/k_A \ll 1$.

B. Characterization of Markovian versus non-Markovian rate processes

We now turn to the Markovian versus non-Markovian nature of the reaction. The general theory of rate presented in the previous section assumes always non-Markovian. On the other hand, the experimental observations appear often Markovian. It is desirable to have a working criterion on the nature of ET kinetics. In contact with experiments, let us consider the scaled population,

$$\Delta(t) \equiv \frac{P_j(t) - P_j(\infty)}{P_j(0) - P_j(\infty)}; \quad j = a, b. \quad (19)$$

It does not depend on the state-index due to the identity of $P_a(t) + P_b(t) = 1$. The simple (Markovian) kinetic rate equation, $\dot{P}_a(t) = -kP_a(t) + k'P_b(t)$, can be represented in terms of the scaled population as

$$\dot{\Delta}_{\text{Mar}}(t) = -w\Delta_{\text{Mar}}(t). \quad (20)$$

The involving decay constant, $w = k + k'$, could be measured readily, if the rate does behave like Markovian. The forward and backward reaction rate constants can then be evaluated as $k = wK_{\text{eq}}/(1 + K_{\text{eq}})$ and $k' = w/(1 + K_{\text{eq}})$, respectively.

A non-Markovian rate process can be described by the *kinetic rate memory kernel* $\hat{w}(t - \tau)$ via

$$\dot{\Delta}(t) \equiv - \int_0^t d\tau \hat{w}(t - \tau) \Delta(\tau). \quad (21)$$

In other words, one can deduce the rate kernel from the population evolution as $\hat{w}(t) = L^{-1}\{[1 - s\tilde{\Delta}(s)]/\tilde{\Delta}(s)\}$. Here $\tilde{\Delta}(s)$ denotes the Laplace transform of $\Delta(t)$, while $L^{-1}\{\cdot\}$ the inverse Laplace transform, i.e.

$$w(s) \equiv L\{\hat{w}(t)\} \equiv \int_0^\infty dt e^{-st} \hat{w}(t) = \frac{1 - s\tilde{\Delta}(s)}{\tilde{\Delta}(s)}. \quad (22)$$

In Appendix B, we present the explicit expression of $w(s)$ in terms of $k(s)$ and $k'(s)$; see eq B7, together with some useful identities in relation to the Laplace transform. Unlike $w(s)$, the population evolution alone is in general not sufficient to determine both $k(s)$ and $k'(s)$.

Equivalent to the kinetic rate kernel $\hat{w}(t)$ defined in eq 21, one may also define the time-local rate $W(t)$ via $\dot{\Delta}(t) = -W(t)\Delta(t)$. Note that while the kernel $\hat{w}(t)$ is always well behaved, its time-local counterpart, $W(t) = -\dot{\Delta}(t)/\Delta(t)$, may diverge at certain time, say t' , due to the possibility of $\Delta(t') = 0$ in an underdamped non-Markovian rate process. At time t' , the effective kinetics reduces to the zero-order rate process, since $W(t')\Delta(t')$ remains finite. Moreover, eq 21 implies also that $W(t=0) = 0$ and $W(t \rightarrow \infty) = w(s=0) \equiv w_0$. The latter is nothing but the fact that long-time regime is Markovian.

To determine the short-time behavior for the population dynamics, we notice the identity,

$$\hat{k}(t=0) = \hat{k}'(t=0) = 2V^2/\hbar^2. \quad (23)$$

This can be obtained directly by considering the fact that the short-time behavior is identical to $\hat{k}_{\text{NA}}(t=0)$ (cf. eq 16), regardless whether the reaction is nonadiabatic or not. Together with eq B8, and setting $P_a(0) = 1$, we obtain

$$\hat{w} \equiv \hat{w}(t=0) = \frac{2V^2}{\hbar^2} \frac{1 + K_{\text{eq}}}{K_{\text{eq}}}. \quad (24)$$

It determines the short-time behavior of the scaled population dynamics, as $\dot{\Delta}(0) = 0$ and $\ddot{\Delta}(0) = -\hat{w}$ that are implied in eq 21.

The short- and long-time behavior described above can be summarized as

$$\Delta(t \rightarrow 0) \approx e^{-\hat{w}t^2/2}, \quad \Delta(t \rightarrow \infty) \approx e^{-wt}. \quad (25)$$

Besides the above asymptotic behaviors, $\Delta(t)$ is in general also influenced by the coherent motion or quantum beat, as long as the rate process goes beyond the second-order in the transfer coupling V . As the asymptotic behaviors are concerned, it may suggest to use the Kubo's line shape function,³²

$$\Delta_K(t) = \exp \left[-\kappa^{-2} (e^{-\hat{w}t/w} - 1 + \hat{w}t/w) \right], \quad (26)$$

to analyze the nature of population transfer dynamics. The involving Kubo's Markovianicity parameter is (cf. eqs 24 and 25)

$$\kappa \equiv \frac{\hat{w}^{1/2}}{w} = \left(\frac{2K_{\text{eq}}}{1 + K_{\text{eq}}} \right)^{1/2} \frac{V}{\hbar k}. \quad (27)$$

The rate process assumes Markovian or non-Markovian, when $\kappa > 1$ or $\kappa < 1$, respectively.

IV. EFFECTS OF QUANTUM SOLVATION: NUMERICAL RESULTS AND DISCUSSIONS

A. Debye solvent model and general remarks

For the numerical demonstrations presented hereafter, we consider the ET system in eq 1 or Fig. 1, with the solvation correlation function in eq 5 being characterized by

$$C(t) = \eta \exp(-t/\tau_L). \quad (28)$$

This is the Debye solvent model, with the longitudinal relaxation time τ_L and the pre-exponential parameter^{25,33}

$$\eta = \lambda(2k_B T - i\hbar/\tau_L). \quad (29)$$

For the above ET system, the analytical expressions for the reduced density matrix $\rho(t)$ and the involving dynamics rate functions, $k(s)$ and $k'(s)$, have all been constructed in Ref. 25. Note that eq 28 satisfies a semiclassical fluctuation-dissipation theorem, valid when the temperature is comparable with or higher than the system's transition energy.^{25,34} This is the only approximation involved in this paper.

To elucidate the quantum solvation effect on ET, especially as the reaction mechanism is concerned, the rate in the classical solvation limit will also be evaluated as a reference. The classical solvation correlation function assumes real; i.e., $\eta \rightarrow \eta_{\text{cl}} = 2\lambda k_B T$ when $k_B T/\hbar \gg \tau_L^{-1}$. It follows $|\eta - \eta_{\text{cl}}|/\eta_{\text{cl}} = 0.5\tau_{\text{ther}}/\tau_L$, with $\tau_{\text{ther}} \equiv \hbar/(k_B T)$ denoting the *thermal time* ($\tau_{\text{ther}} = 26$ fs for $T = 298$ K). The quantum solvation effect can be significant when $\tau_L < \tau_{\text{ther}}$.

It is also noticed that the solvation longitudinal relaxation time τ_L is proportional to the solvent viscosity.^{14,15} In this sense, the k versus τ_L behavior can be referred as the *rate-viscosity* character. This connection suggests the well-established Kramers' picture of the solvation effect on chemical reaction^{28,29} be exploited in the following to elucidate the underlying ET reaction mechanism.

B. Quantum vs. classical solvation effects

As the mechanism is concerned, the effect of quantum versus classical solvation is expected to be most distinct in the following two scenarios (cf. Fig. 1). One is the symmetric ET system ($E^\circ = 0$) in which the Fermi resonance enhanced quantum tunneling is anticipated. Another is the classical barrierless system ($E^\circ + \lambda = 0$) where the Marcus' inversion takes place. Figure 2 depicts the evaluated rate-viscosity characteristics for these two scenarios of ET system, at two values of transfer coupling: $V = 1$ kJ/mol (upper-panels) and $V = 0.01$ kJ/mol (lower-panels). The solvation energy $\lambda = 3$ kJ/mol and temperature $T = 298$ K.

In the high-viscosity ($\tau_L > \tau_{\text{ther}}$) regime, the difference between the quantum (solid-curve) and the classical (dashed-curve) in each panel diminishes (at the qualitative level). This observation is consistent with the physical picture that the high viscosity (or slow motion) implies a large effective mass and thus leads to the classical solvation limit. Observed here is also the Kramers' fall-off behavior^{28,29} for the adiabatic rates in the upper panels. This is the diffusion limit; the higher the solvent viscosity is, the more backscattering (or barrier re-crossing in the classical sense) events will be. For the nonadiabatic processes in the lower panels, the backscattering effects are quenched. This accounts for the plateau, observed in the lower-panel (c) or (d), at which the Marcus' nonadiabatic ET regime is reached, and the rate becomes independent of viscosity.

In the low-viscosity ($\tau_L < \tau_{\text{ther}}$) regime, the difference between quantum and classical solvation is at the mechanism level for the two specified types of ET systems. For the symmetric ($E^\circ = 0$) system [the left-panel (a) or (c) of Fig. 2], the quantum rates (solid-curves) are apparently Fermi resonance-assisted tunneling dominated processes, while the classical rates (dash-curves) are barrier crossing events. In contrast to that $k \gg k_{\text{cl}}$ in the $\tau_L < \tau_{\text{ther}}$ regime for the symmetric ($E^\circ = 0$) system, observed is the opposite result of $k \ll k_{\text{cl}}$ for the Marcus' barrierless ($E^\circ + \lambda = 0$) system [the right-panel (b) or (d) of Fig. 2]. In the latter case, the classical rate does behave as a barrierless reaction, but the quantum rate exhibits the Kramers' barrier-crossing characteristics as a function of viscosity. This may indicate that for the ET in the classical barrierless system there is an effective viscosity-dependent barrier that vanishes as τ_L increases. In other words, the barrier of $(E^\circ + \lambda)^2/(4\lambda)$, as depicted in the ET schematics Fig. 1, is the static picture that

assumes the solvation potential being fixed. This picture is valid in the high-viscosity (or slow-modulation) regime, but no longer true in the low-viscosity (or fast-modulation) regime. In general, the effective solvation potential for ET reaction is solvent viscosity dependent.

To confirm the above observed ET mechanism-related features, the values of λ and T are varied, and the results for $V = 1$ kJ/mol are summarized in Fig. 3. Here, k/k_{cl} as functions of $\tau_L/\tau_{\text{ther}}$ are depicted. This figure verifies that $\tau_L/\tau_{\text{ther}}$ does serve a proper measure for the nature of solvation. The reaction mechanism turnover occurs at $\tau_L = \tau_{\text{ther}}$, for the symmetric ($E^\circ = 0$) case, and classical barrierless ($E^\circ + \lambda = 0$) ET systems. In the former case, it is changed from the tunneling to barrier-crossing, while in the latter case from the barrier-crossing to barrierless ET rate process.

Let us now consider the Marcus-type inversion behaviors. Figure 4 presents the Marcus-plots, the logarithmic rate $\log k$ versus reaction endothermicity E° , in relation to Fig. 2. Three values of $\tau_L/\tau_{\text{ther}}$ are chosen as 0.1 (solid-curves), 1 (dot-curves), and 10 (dash-curves), to represent the low-, intermediate-, and high-viscosity regimes, respectively.

Note that $E^\circ = -\lambda$ does represent the classical barrierless ET systems in all cases in study. All the classical rates [right-panels, Fig. 4(b) and (d)] have inversions occurring at $E^\circ = -\lambda$. Moreover, all of them are symmetric about $E^\circ = -\lambda$. The Marcus' parabolic character is recovered in the high-viscosity, nonadiabatic and classical limit, and is practically the dashed curve in Fig. 4(d).

The quantum rates depicted in the left-panels [Fig. 4(a) and (c)] also show inversion behavior. However, the observed inversion region depends sensitively on the solvent viscosity, and shows also an asymmetric character that will be elaborated soon. Apparently, the quantum rate inversion region is closely related to the interplay between the barrier-crossing and tunneling processes.

Let us start with Fig. 4(a). Consider first the high-viscosity regime, in which, according to the analysis made earlier for Fig. 2, the ET process is qualitatively the same as its classical counterpart. Consequently the dash-curve in Fig. 4(a) has the inversion region around the classical barrierless position at $E^\circ = -\lambda$. Consider now the low-viscosity regime, in which, again, according to the analysis earlier there is always a nonzero barrier for the ET reaction, covering over the entire range of E° including the value of $E^\circ = -\lambda$. This explains the inversion behavior of the solid curve of Fig. 4(a) that is peaked at the resonant position of $E^\circ = 0$. As the viscosity increases, the inversion region smoothly shifts from the resonant peak position $E^\circ = 0$ to the classical barrierless position of $E^\circ = -\lambda$.

To explain the asymmetric property of the quantum inversion behavior as depicted in the left panels of Fig. 4, recall that $k(-E^\circ) \approx k'(E^\circ)$, the backward reaction rate, and $k(E^\circ) < k'(E^\circ)$ for an endothermic ($E^\circ > 0$) reaction. This leads immediately to the asymmetric property of the solid-curve in Fig. 4(a) or (c), in which the blue

(endothermic) wing falls off faster than its red (exothermic) wing. This asymmetry decreases as the viscosity increases, since the high viscosity regime behaves classically.

V. THE ADIABATIC AND MARKOVIAN CHARACTERS OF THE REACTION

We are now in the position to demonstrate (for the cases of quantum solvation only) the issues in relation to the nature of ET rate process, as addressed in Sec. III. Let us start with the adiabatic/nonadiabatic character depicted in Fig. 5. Here, each individual k (thin)-curves, as function of τ_L , is decomposed into its adiabatic k_A and nonadiabatic k_{NA} components (eq 18). These two components are given in the upper-panel [Fig. 5(a) or (b)] and the lower-panel [Fig. 5(c) or (d)], respectively. The left-panels are for the $E^\circ = 0$ system [Fig. 5(a) and (c)], while the right-panels are for the $E^\circ + \lambda = 0$ system [Fig. 5(b) and (d)]. In each panel, four values of transfer coupling are used: $V/(\text{kJ/mol}) = 0.25$ (dotted), 0.5 (dashed), 1 (solid), and 2 (dash-dotted).

It is observed that in the low-viscosity ($\tau_L < \tau_{\text{ther}}$) regime, the reaction is nonadiabatic; see Fig. 5(c) and (d). This observation may be understood as follows. In the low-viscosity regime, the solvent fluctuates fast and stabilizes the ET system in the acceptor state before backscattering taking place. As results, the reaction is nonadiabatic in the low-viscosity regime, at least for the range of transfer coupling strength considered here. The above picture is also consistent with the observation that in the diffusion ($\tau_L \gg \tau_{\text{ther}}$) limit, where $k \propto 1/\tau_L$, the reaction assumes an adiabatic rate process; see Fig. 5(a) and (b).

Figure 6 presents the adiabaticity parameters, k_{NA}/k_A , as function of reaction endothermicity E° , at $V = 1$ kJ/mol, with the three specified values of $\tau_L/\tau_{\text{ther}} = 0.1$, 1, and 10. The inverse of these values are also used individually to scale the corresponding adiabaticity curves, as depicted in Fig. 6. The adiabaticity curve in high-viscosity ($\tau_L/\tau_{\text{ther}} = 10$) regime looks all normal, being of the minimum about where the rate maximum is; cf. the dash-curve in Fig. 4(a). The faster the ET passage, the less adiabatic (or more surface-hopping) the reaction would be. This feature remains largely unchanged in the intermediate-viscosity ($\tau_L/\tau_{\text{ther}} = 1$) case, except for that the adiabaticity minimum now is slightly *negative*, or $k > k_{NA}$. It contradicts with the argument made earlier for eq 18. The abnormality here may be accounted for, at least partially, by the associated tunneling rate process, as elaborated below.

The abnormality in the adiabaticity parameter is most striking around the symmetric ($E^\circ \approx 0$) system in the low-viscosity ($\tau_L/\tau_{\text{ther}} = 0.1$) regime. This is tunneling dominant scenario, as discussed in Sec. IV. Considered here is also the strong transfer coupling case of $V = 1$ kJ/mol. Thus, the observed abnormality is most

likely caused by the coherent ET reaction. The argument for $k < k_{NA}$, due to the backscattering-induced total rate reduction, may no longer be valid. Moreover, we will see soon that the ET reaction in the observed abnormal region is non-Markovian, leading to the rate constant description inadequate at all; see Fig. 10 and the comments there.

We now turn to the Markovian/non-Markovian nature of ET reaction. The key quantity here is the Markovianity parameter κ (eq 27). It involves the reaction rate k and the equilibrium constant K_{eq} . The detailed knowledge on how K_{eq} depends on the Debye solvent parameters can be found in Ref. 25. For the rate in the low-viscosity regime, $k \approx k_{NA}$, as depicted in the lower-panels of Fig. 5, resulting in $k \approx 2V^2\Gamma/(E^{\circ 2} + \Gamma^2)$, with $\Gamma = 2\lambda k_B T \tau_L$ for the Debye solvent model in study; cf. eq 16 with eq 28. Thus,

$$\kappa \approx \lambda k_B T \tau_L / V; \quad \text{when } E^\circ = 0 \text{ and } \tau_L < \tau_{\text{ther}}. \quad (30)$$

This equation can be used to estimate the Markovianity parameter for a symmetric ET system ($E^\circ = 0$, implying also $K_{\text{eq}} = 1$) in the low-viscosity regime.

Figure 7 shows the evaluated Markovianity κ (eq 27) as function of $\tau_L/\tau_{\text{ther}}$, for the same ET systems as Fig. 2 (without the classical solvation parts). For $E^\circ + \lambda = 0$ (lower-panel), the ET rate process behaves Markovian ($\kappa > 1$), even for the strong transfer coupling ($V = 1$ kJ/mol) case. Apparently, the non-Markovian ($\kappa < 1$) rate process is most likely to occur in the Fermi-resonance tunneling regime, where $E^\circ = 0$ and $\tau_L < \tau_{\text{ther}}$, with the approximated expression of κ given in eq 30. The above comments are further confirmed by Fig. 8, in which the Markovianity κ is plotted as function of E° , at the three representing values of $\tau_L/\tau_{\text{ther}}$.

Figure 9 depicts the scaled population evolution, $\Delta(t)$ (eq 19), for the ET systems of $E^\circ = 0$ (three left-panels) and $E^\circ + \lambda = 0$ (three right-panels). The upper [(a) and (b)], middle [(c) and (d)], and lower [(e) and (f)] panels are of the specified values of viscosity, $\tau_L/\tau_{\text{ther}} = 0.1$, 1 and 10, respectively. The transfer coupling strength is $V = 1$ kJ/mol. The weak transfer coupling ($V = 0.01$ kJ/mol) counterparts, as depicted in the inserts of individual panels, are shown all Markovian, with $\kappa \gg 1$ for their values of Markovianity; cf. Fig. 7 and Fig. 8. Included for comparison in each panel are also the Kubo's $\Delta_K(t)$ (eq 26) and Markovian $\Delta_{\text{Mar}} = \exp(-wt)$ counterparts, where $w = k + k'$. As the envelop of population evolution is concerned, the significant non-Markovian nature is only observed in Fig. 9(a), with the relevant part is enlarged in Fig. 10. This is a symmetric ET system in the strong transfer ($V = 1$ kJ/mol) coupling and low-viscosity ($\tau_L/\tau_{\text{ther}} = 0.1$) regime. The corresponding Markovianity value ($\kappa = 0.3$) is found to agree well with the aforementioned approximate expression of eq 30.

VI. CONCLUDING REMARKS

The quantum solvation, adiabatic/nonadiabatic and Markovian/non-Markovian characters are important issues in understanding chemical reaction, including ET in solution. Here, we have revisited these issues in a unified and transparent manner, with the aid of Debye solvent model (eq 28) that supports an analytical solution without additional approximations.²⁵ The physical picture discussed in this work is however rather general.

We have presented a full account for the effect of quantum solvation on the ET rate process (Sec. IV). Not just can it change a barrier-crossing event to tunnelling, the quantum nature of solvent can also lead a classical barrierless reaction to an effective barrier-crossing rate process. The resulting rate may differ from its classical counterpart by order of magnitude. The quantum solvation is found to be distinctly important in low-viscosity (fast-modulation) solvents. For a realistic solvent that consists of multiple correlation time scales, only the slow-modulation solvent modes can be treated classically.

The adiabatic-nonadiabatic decomposition of rate (eq 18) is practically useful, provided that the total rate k can be experimentally measured and the nonadiabatic rate k_{NA} can be readily evaluated via eq 16. The adiabaticity parameter $k_{\text{NA}}/k_{\text{A}} = k_{\text{NA}}/k - 1$, as inferred from eq 18, can then be used to discuss the adiabatic/nonadiabatic nature of reaction. Interestingly, a negative adiabaticity may indicate there is a certain degree of quantum tunneling taking place; cf. Fig. 6 and its comments.

We have also proposed to use the Markovianity parameter κ (eq 27), based on the Kubo's motional narrowing function, for analyzing the Markovian/non-Markovian nature of electron transfer rate process. Note the solvent relaxation time scale is typically in the order of picosecond, while τ_{ther} for room temperature is 26 fs. This amounts to the high-viscosity or slow-modulation regime of present studies on ET. The resulting Markovianity parameter, as depicted in Fig. 7 and Fig. 8, is typically of $\kappa > 1$ for the aforementioned typical cases. This may account for why most experimental observations do support the Markovian ($\kappa > 1$) rate constant description.

We have pointed out that a non-Markovian rate process is most likely to occur in the symmetric ET system at the fast-modulation regime. It is just the opposite to the spectroscopic case. According to the motional narrowing picture, the fast modulation leads to a Markovian spectroscopic process.^{31,32} The above seemingly counter-intuitive phenomenon in relation to the nature of rate process may be understood as follows. First of all, the motional narrowing picture is applicable to the spectrum of rate kernel, rather than the population evolution itself. The narrower the rate kernel spectrum is, the less Markovian of rate process would be. However, this is not the complete picture. The peak position of the rate kernel spectrum, in relation to where rate constant is eval-

uated, should also be considered. It shifts from the classical Marcus' inversion position at $E^\circ = -\lambda$ in the slow-modulation limit, to the quantum resonant tunneling at $E^\circ = 0$ in the fast-modulation (or motional-narrowing) regime, see Fig. 4 (left-panels). Equation (30) that is achieved at $E^\circ = 0$ can be considered as the lower bound of the Markovianity κ for the ET rate process. In the fast modulation regime. In this regime, the population transfer may also exhibit the quantum beat feature that is non-Markovian in a strict sense. We shall investigate these complex cases elsewhere.

Acknowledgments

Support from the RGC Hong Kong (604006), NNSF of China (50121202), and National Basic Research Program of China (2006CB922004) is acknowledged. R. X. Xu would also like to thank the support from the NNSF of China (20403016 and 20533060) and Ministry of Education of China (NCET-05-0546).

APPENDIX A: PERTURBATIVE RATE KERNELS

In this appendix, we shall treat the nonadiabatic rate problem, on the basis of the standard perturbation theory on the reduced density matrix $\rho(t)$, assuming the transfer coupling last term of eq 1, is weak. At the initial time $t = 0$, the total composite density operator is $\rho_{\text{T}}(0) = \rho_a^{\text{eq}}|a\rangle\langle a|$. Consider eq 8 for the coherence components, which for the two-level ET system reads explicitly as (setting $\hbar = 1$ in this appendix)

$$\alpha \tilde{\rho}_{ba} = -iV(\tilde{P}_a - \tilde{P}_b) - z\tilde{P}_b - y\tilde{\rho}_{ba}^*. \quad (\text{A1})$$

Here $\alpha = s + i(E^\circ + \lambda) + x$, and

$$x \equiv \Pi_{ba,ba}, \quad y \equiv \Pi_{ba,ab}, \quad z \equiv \Pi_{ba,bb}. \quad (\text{A2})$$

Combining the initial condition $P_a(t=0) = 1$ and the perturbative action of \hat{V} together result immediately in $\tilde{P}_a^{\{0\}} = 1/s$ and

$$0 = \tilde{P}_a^{\{2k+1\}} = \rho_{ba}^{\{2k\}} = \alpha^{\{2k+1\}} = y^{\{0\}} = y^{\{2k+1\}} = z^{\{2k\}}.$$

Therefore, the lowest order in eq A1 reads

$$\alpha^{\{0\}} \tilde{\rho}_{ba}^{\{1\}} = -iV/s. \quad (\text{A3})$$

On the other hand, the standard first-order perturbative expression is

$$\rho_{ba}^{(1)}(t) = -iV \int_0^t d\tau \exp[-g(\tau)]. \quad (\text{A4})$$

Here

$$\exp[-g(t)] = \left\langle \exp_+ \left\{ -i \int_0^t d\tau [E^\circ + U(\tau)] \right\} \right\rangle. \quad (\text{A5})$$

Using the second-cumulant expansion expression, which is exact for the Gaussian solvation process, results in

$$g(t) = i(E^\circ + \lambda)t + \int_0^t d\tau \int_0^\tau d\tau' C(\tau'). \quad (\text{A6})$$

We have then

$$s\rho_{ba}^{\{1\}}(s) = -iVL\{\exp[-g(t)]\} \equiv -iVJ(s). \quad (\text{A7})$$

Together with eq A3, we obtain

$$\alpha^{\{0\}}(s) = 1/J(s). \quad (\text{A8})$$

Together with $y^{\{0\}} = 0$, eq 15a to the lowest order reads $k_{\text{NA}}(s) = (2V^2/\hbar^2)\text{Re}J(s)$, where $J(s)$ denotes the Laplace transform of $\exp[-g(t)]$ (cf. eq A7). We obtain therefore eq 16.

APPENDIX B: SOME USEFUL RELATIONS FOR RATES

Let us first present some basic relations in connection to the Laplace transform, defined for $s \geq 0$ as

$$\tilde{f}(s) \equiv L\{f(t)\} \equiv \int_0^\infty dt e^{-st} f(t). \quad (\text{B1})$$

It satisfies the boundary condition, $L\{\cdot\}|_{s \rightarrow \infty} = 0$, and

$$L\left\{\int_0^t d\tau f_1(t-\tau)f_2(\tau)\right\} = \tilde{f}_1(s)\tilde{f}_2(s), \quad (\text{B2})$$

$$L\{\dot{f}(t)\} = s\tilde{f}(s) - f(0). \quad (\text{B3})$$

Using eq B3, together with the identities of $L\{\cdot\}|_{s \rightarrow \infty} = 0$ and $L\{\dot{f}(t)\}|_{s=0} = f(\infty) - f(0)$, we obtain immediately

$$f(0) = \lim_{s \rightarrow \infty} [s\tilde{f}(s)], \quad f(\infty) = \lim_{s \rightarrow 0} [s\tilde{f}(s)]. \quad (\text{B4})$$

We are now in the position to derive some useful relations between the non-Markovian rate variables appearing in Sec. II. From eq 11 and $P_a(t) + P_b(t) = 1$, we have

$$\tilde{P}_a(s) = \frac{P_a(0) + k'(s)/s}{s + k(s) + k'(s)}. \quad (\text{B5})$$

From eqs 19 and 22, we have

$$\tilde{\Delta}(s) = \frac{\tilde{P}_a(s) - P_a(\infty)/s}{P_a(0) - P_a(\infty)} = \frac{1}{s + w(s)}. \quad (\text{B6})$$

The above two equations lead to

$$w(s) = \frac{s[P_a(0)k(s) - P_b(0)k'(s)]}{s[P_a(0) - P_a(\infty)] - P_a(\infty)k(s) + P_b(\infty)k'(s)}. \quad (\text{B7})$$

Together with the first identity of eq B4, we have

$$\hat{w}(t=0) = \frac{P_a(0)\hat{k}(t=0) - P_b(0)\hat{k}'(t=0)}{P_a(0) - P_a(\infty)}. \quad (\text{B8})$$

The above relation will be used in deriving eq 24.

* Electronic address: rxu@ustc.edu.cn; yyan@ust.hk

¹ Marcus, R. A. *J. Chem. Phys.* **1956**, *24*, 966.

² Marcus, R. A. *Annu. Rev. Phys. Chem.* **1964**, *15*, 155.

³ Marcus, R. A. and Sutin, N. *Biochim. Biophys. Acta* **1985**, *811*, 265.

⁴ Kestner, N. R., Logan, J., and Jortner, J. *J. Phys. Chem.* **1974**, *78*, 2148.

⁵ Jortner, J. *Biochim. Biophys. Acta* **1980**, *594*, 193.

⁶ Zusman, L. D. *Chem. Phys.* **1980**, *49*, 295.

⁷ Zusman, L. D. *Chem. Phys.* **1983**, *80*, 29.

⁸ Garg, A., Onuchic, J. N., and Ambegaokar, V. *J. Chem. Phys.* **1985**, *83*, 4491.

⁹ Frauenfelder, H. and Wolynes, P. G. *Science* **1985**, *229*, 337.

¹⁰ Wolynes, P. G. *J. Chem. Phys.* **1987**, *86*, 1957.

¹¹ Sparpagione, M. and Mukamel, S. *J. Phys. Chem.* **1987**, *91*, 3938.

¹² Sparpagione, M. and Mukamel, S. *J. Chem. Phys.* **1988**, *88*, 3263.

¹³ Sparpagione, M. and Mukamel, S. *J. Chem. Phys.* **1988**, *88*, 4300.

¹⁴ Yan, Y. J., Sparpagione, M., and Mukamel, S. *J. Phys. Chem.* **1988**, *92*, 4842.

¹⁵ Yan, Y. J. and Mukamel, S. *J. Phys. Chem.* **1989**, *93*, 6991.

¹⁶ Mukamel, S. and Yan, Y. J. *Acc. Chem. Res.* **1989**, *22*, 301.

¹⁷ Yang, D. Y. and Sheu, S. Y. *J. Chem. Phys.* **1997**, *107*, 9361.

¹⁸ Tang, J. and Lin, S. H. *Chem. Phys. Lett.* **1996**, *254*, 6.

¹⁹ Tang, J. and Lin, S. H. *J. Chem. Phys.* **1997**, *107*, 3485.

²⁰ Rips, I. and Jortner, J. *Chem. Phys. Lett.* **1987**, *133*, 411.

²¹ Bixon, M. and Jortner, J. *Adv. Chem. Phys.* **1999**, *106*, 35.

²² Xu, R. X., Cui, P., Li, X. Q., Mo, Y., and Yan, Y. J. *J. Chem. Phys.* **2005**, *122*, 041103.

²³ Xu, R. X. and Yan, Y. J. *Phys. Rev. E* **2007**, *75*, 031107.

²⁴ Jin, J. S., Welack, S., Luo, J. Y., Li, X. Q., Cui, P., Xu, R. X., and Yan, Y. J. *J. Chem. Phys.* **2007**, *126*, 134113.

²⁵ Han, P., Xu, R. X., Li, B. Q., Xu, J., Cui, P., Mo, Y., and Yan, Y. J. *J. Phys. Chem. B* **2006**, *110*, 11438.

²⁶ Han, P., Xu, R. X., Cui, P., Mo, Y., He, G. Z., and Yan, Y. J. *J. Theor. Comput. Chem.* **2006**, *5*, 685.

²⁷ Nitzan, A. *Chemical Dynamics in Condensed Phases: Relaxation, Transfer and Reactions in Condensed Molecular Systems*; Oxford University Press: New York, 2006.

²⁸ Kramers, H. A. *Physica (Amsterdam)* **1940**, *7*, 284.

²⁹ Hänggi, P., Talkner, P., and Borkovec, M. *Rev. Mod. Phys.* **1990**, *62*, 251.

³⁰ Hynes, J. T. *Annu. Rev. Phys. Chem.* **1985**, *36*, 573.

- ³¹ Kubo, R. *Rep. Prog. Phys.* **1966**, 29, 255.
- ³² Kubo, R. *Adv. Chem. Phys.* **1969**, 15, 101.
- ³³ Tanimura, Y. and Kubo, R. *J. Phys. Soc. Jpn.* **1989**, 58, 101.
- ³⁴ Tanimura, Y. *J. Phys. Soc. Jpn.* **2006**, 75, 082001.

FIG. 1: Schematics of solvent potentials V_a and V_b for the ET system in the donor and acceptor states, respectively, as functions of the solvation coordinate $U \equiv h_b - h_a = V_b - V_a - E^\circ$, with E° being the ET endothermicity and $\lambda = \langle U \rangle$ the solvation energy. The classical barrierless system is that of $E^\circ + \lambda = 0$.

FIG. 2: Electron transfer rate k (solid-curves), as function of solvent longitudinal relaxation time τ_L , with $\lambda = 3$ kJ/mol at $T = 298$ K. Left-panels (a) and (c): $E^\circ = 0$; right-panels (b) and (d): $E^\circ + \lambda = 0$; upper-panels (a) and (b): $V = 1$ kJ/mol; lower-panels (c) and (d): $V = 0.01$ kJ/mol. Included in each panel is also the classical solvation counterpart k_{cl} (dash-curves). Note that $\tau_{ther} \equiv \hbar/(k_B T) = 10^{-1.6}$ ps.

FIG. 3: The ratio of quantum versus classical rates, k/k_{cl} , as function of τ_L/τ_{ther} , with the transfer coupling $V = 1$ kJ/mol, at various specified values of λ and T .

FIG. 4: The rate k (left-panels) and the classical counterpart k_{cl} (right-panels), as function of E° , with $\lambda = 3$ kJ/mol at $T = 298$ K; upper-panels (a) and (b): $V = 1$ kJ/mol; lower-panels (c) and (d): $V = 0.01$ kJ/mol. The three values of relative relaxation time scale, $\tau_L/\tau_{ther} = 0.1$ (solid), 1 (dotted), and 10 (dashed) are chosen to represent the low, intermediate, and high-viscosity regimes, respectively.

FIG. 5: The decomposition of rate k (thin-curves), following eq 18, into the adiabatic k_A (upper-panels) and nonadiabatic k_{NA} (lower-panels) components, and plotted as functions of τ_L/τ_{ther} , with $\lambda = 3$ kJ/mol and $T = 298$ K. Left-panels (a) and (c): $E^\circ = 0$; right-panels (b) and (d): $E^\circ + \lambda = 0$. Each panel involves four values of transfer coupling strength: $V/(kJ/mol) = 0.25$ (dotted), 0.5 (dashed), 1 (solid), and 2 (dash-dotted), respectively.

FIG. 6: The adiabaticity k_{NA}/k_A as function of E° , for $\tau_L/\tau_{ther} = 10, 1$ and 0.1 . The inverse of τ_L/τ_{ther} is also used to the scale individual adiabaticity curve. $V = 1$ kJ/mol, $\lambda = 3$ kJ/mol, and $T = 298$ K.

FIG. 7: The Markovianicity parameter κ (eq 27), as function of τ_L/τ_{ther} , at $V = 1$ kJ/mol (solid) and 0.01 kJ/mol (dashed), with $\lambda = 3$ kJ/mol and $T = 298$ K, for (a) $E^\circ = 0$ and (b) $E^\circ + \lambda = 0$.

FIG. 8: The Markovianicity parameter κ (eq 27) as the function of E° , with $\lambda = 3$ kJ/mol and $T = 298$ K, at $\tau_L/\tau_{ther} = 0.1$ (solid), 1 (dotted) and 10 (dashed): (a) $V = 1$ kJ/mol and (b) $V = 0.01$ kJ/mol.

FIG. 9: The scaled population $\Delta(t)$ (eq 19) evolution, evaluated at $\tau_L/\tau_{ther} = 0.1$ (upper-panels), 1 (middle-panels), and 10 (lower-panels); Left-panels: $E^\circ = 0$; right-panels: $E^\circ + \lambda = 0$. Here, $V = 1$ kJ/mol, $\lambda = 3$ kJ/mol, and $T = 298$ K. Included in each panel are also the corresponding Kubo's $\Delta_K(t)$ (eq 26; dashed) and Markovian $\Delta_{Mar}(t)$ (dotted). The insert in each panel is the $V = 0.01$ kJ/mol counterpart, where all these three curves are identical.

FIG. 10: The amplified portion of Fig. 9(a). The scaled population evolution $\Delta(t)$ (solid), Kubo's $\Delta_K(t)$ (dashed), and Markovian $\Delta_{Mar}(t)$ (dotted).

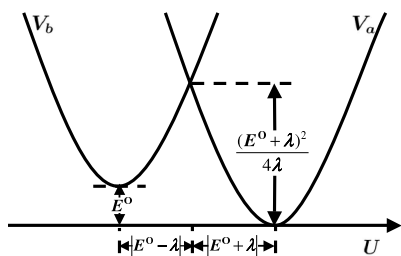


Figure 1

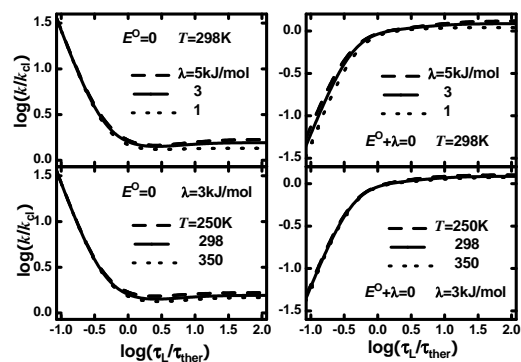


Figure 3

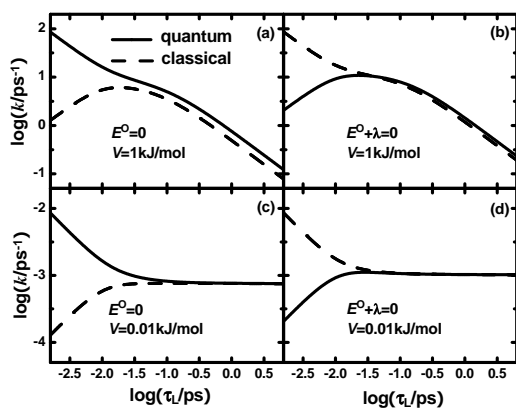


Figure 2

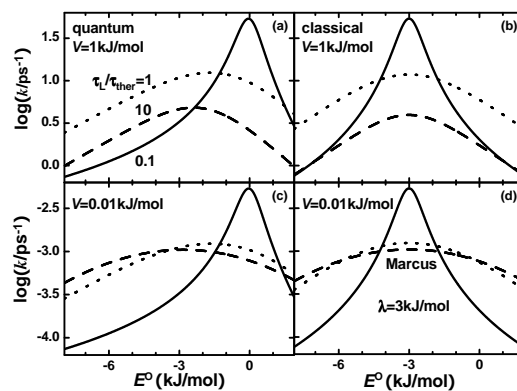


Figure 4

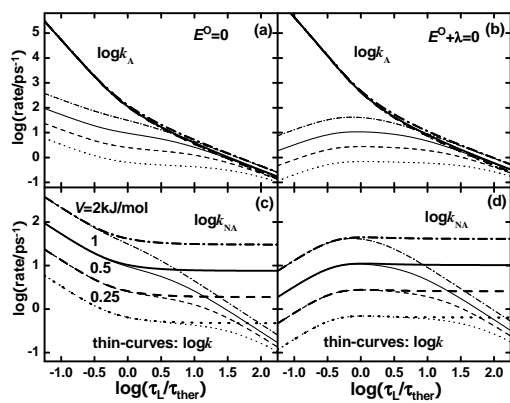


Figure 5

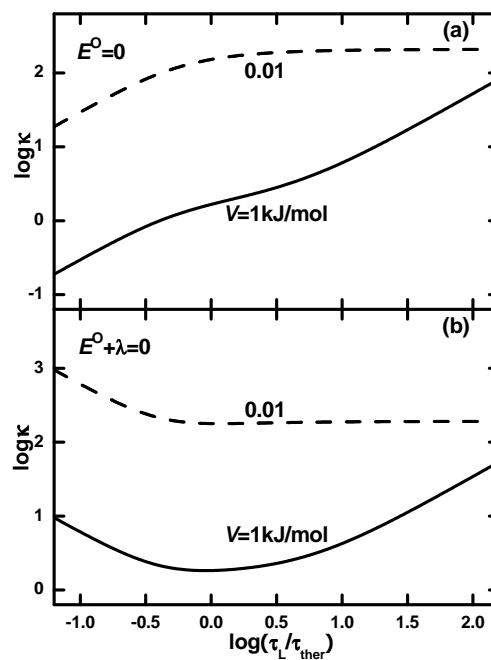


Figure 7

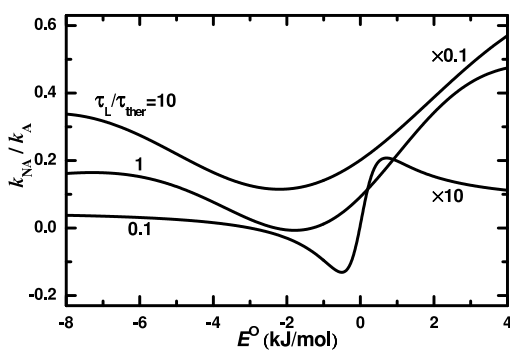


Figure 6

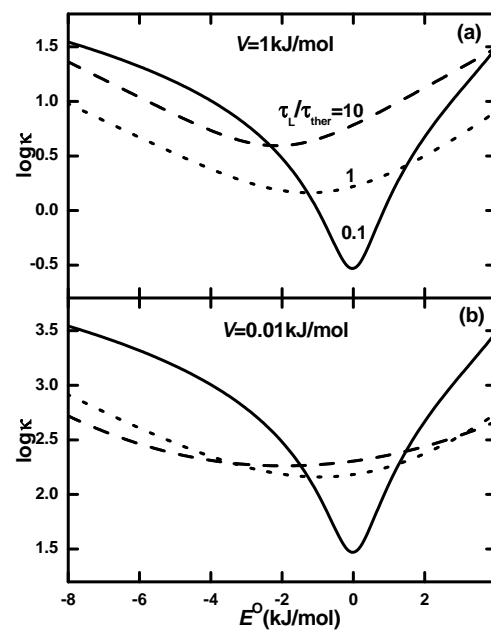


Figure 8

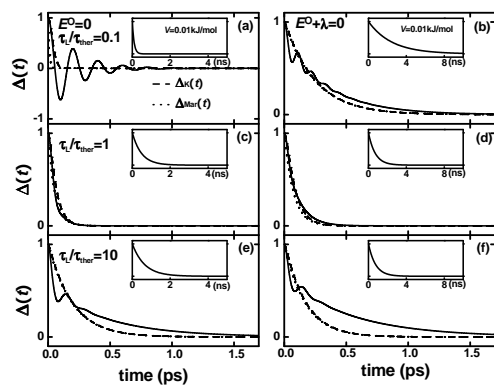


Figure 9

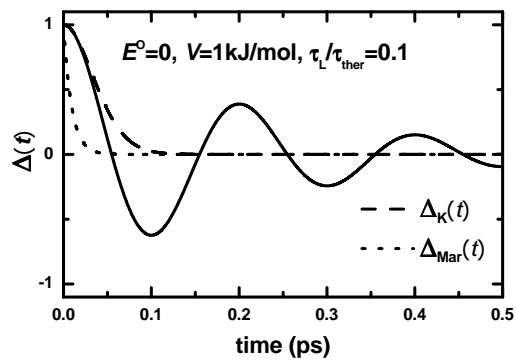


Figure 10